BNL-223596-2022-JAAM

The b-decay of 141Ba

J. Rufino, E. McCutchan

To be published in "Physical Review C"

October 2022

Nuclear Science and Technology Department

Brookhaven National Laboratory

U.S. Department of Energy

USDOE Office of Science (SC), Nuclear Physics (NP) (SC-26)

DISCLAIMER

The β-decay of ^{141}Ba

Javier Rufino Jr[1,2], E.A. McCutchan[2], S. Zhu[2,3], A. A. Sonzogni[2], M. Alcorta[3], P. F. Bertone[3], M. P. Carpenter[3], J. Clark[3], C. R. Hoffman[3], R. V. F. Janssens[4,5], F. G. Kondev[3], T. Lauritsen[3], C. J. Lister[3], R. Pardo[3], A. Rogers[3], G. Savard[3], D. Seweryniak[3] and R. Vondrasek[3]

[1]*Physics and Astronomy, University of Texas at San Antonio, San Antonio, TX 78249*

[2]*National Nuclear Data Center, Brookhaven National Laboratory, Upton, NY 11973-5000*

[3]*Physics Division, Argonne National Laboratory, Argonne, Illinois 60439, USA*

[4]*Department of Physics and Astronomy, University of North Carolina, Chapel Hill, North Carolina 27599, USA and*

[5]*Triangle Universities Nuclear Laboratory, Duke University, Durham, North Carolina 27708, USA*

(Dated: September 9, 2022)

The β-decay strength function of nuclides produced in fission is important as it dictates the distribution of decay energy between electrons, neutrinos and gamma rays and so is critical for calculating decay heat in reactors and for estimating the reactor antineutrino spectrum. Several experimental techniques are available to determine this strength function, including electron spectroscopy, gamma-ray calorimetry (TAGS spectroscopy) and detailed, high-resolution spectroscopy with modern large HPGe arrays. This work investigates the decay of the well-known and strongly produced fission fragment, ^{141}Ba. A beam of ^{141}Cs was implanted at the target position of Gammasphere and the subsequent decay of the daughter ^{141}Ba studied. Extensive decay spectroscopy was possible up to the decay Q-value of 3.197(7) MeV, including a significant extension of the level scheme, and detailed angular correlation measurements for all levels with greater than 0.25 % β feeding. The distribution of β-decay strength was then inferred and compared to previous calorimetric studies. The agreement was excellent and provides a benchmark for comparing strength function methods and data for a more detailed understanding of the structure of ^{141}La.

I. INTRODUCTION

Knowledge of the processes following the β-decay of fission fragments is essential for reactor control, through the delayed neutrons [1], for understanding the post-fission decay heat produced in reactors [2], and for estimating the flux of reactor antineutrinos both for neutrino oscillation physics [3, 4] and for remote monitoring of reactor operation and fuel rod composition [5]. The distribution of β-decay probability with excitation energy, the "Strength Function", is critical for understanding the partition of the decay energy between neutrons, electrons, neutrinos and photons, and so is essential for all these applications. Several techniques have been developed for ascertaining the strength function, including measuring the spectrum of β-decay electrons, using electromagnetic calorimetry, or performing detailed discrete-line gamma spectroscopy using high-resolution HPGe detectors. This paper describes an ultra-high statistics discrete line spectroscopy study of a well-known fission fragment, ^{141}Ba, in order to compare the inferred strength function with that obtained from calorimetry. The current measurement exploits the efficiency and granularity of the Gammasphere array to maximize the information which can be gained. Comparisons between gamma-ray calorimetry measurements and HPGe spectroscopy have been made in the past [6], however, these involved very high Q-value decays. In this specific case, the decay Q-value is relatively low, Q=3.197(7) MeV [7], so the issue of high fragmentation of the gamma decay or "Pandemonium" [8] is modest. An advantage of the discrete-line approach is that it produces a wealth of detailed new spectroscopic information which can be used for testing nuclear models. This includes a determination of the spin of all the states with β-feeding intensity above 0.25% using angular correlation measurements.

In the 1990's, Greenwood *et al.,* [9–11] performed an extensive series of Total Absorption Gamma-ray Spectroscopy (TAGS) measurements in the fission fragment region. While new measurements from the Valencia/Jyvaskyla [12], ORNL MTAS [13] and MSU SuN [14] groups are emerging, the Greenwood *et al.,* measurements are still the benchmark in the decay libraries such as ENDF [15] and JEFF [16]. In the Greenwood *et al.,* seminal TAGS paper [9], the authors provided an extensive discussion of the uncertainties in their measurements and analysis, but did not give errors for their deduced β-feeding intensities, except for the ground state to ground state branch. This leaves a shortfall in the databases which generally need numerical assessments of the experimental uncertainties.

The main motivation for the present work was to perform a high-sensitivity, high-resolution γ-ray measurement to benchmark and complement a Greenwood *et al.,* experiment and try to clarify the issue of accuracy and uncertainty. We chose ^{141}Ba as a strongly-produced fission fragment, with a 5.8% yield in thermal neutron-induced ^{235}U fission, and a 5.1 % yield in thermal neutron-induced ^{239}Pu fission [16]. Knowledge of the level structure of ^{141}La populated in the decay of ^{141}Ba has increased steadily over the years, starting with basic decay schemes constructed from observing individual γ-ray transitions in the 1970's [19, 20]. A decade later, Proto *et al.,* [21] and Faller *et al.,* [22], extended the level scheme through γ-γ coincidence measurements. Ref. [21] additionally performed conversion electron spectroscopy to help determine the multipolarities of low-energy transitions. The current NNDC data evaluation [25] adopts the measurement of Faller *et al.,* [22], while including a few of the unplaced transi-

tions from Ref. [21]. The Greenwood *et al.,* measurement [9] provided a description of the β-feeding strength to individual excited states, but relied on the existing discrete line decay scheme.

An additional benefit of the discrete line method is that it provides a wealth of new data to help understand the level structure of ^{141}La, which lies in the transitional region above neutron number N=82 where prolate deformation and octupole collectivity start to emerge. The ground state of ^{141}Ba has the N=85 neutron in a state based on the N=5 $\nu f_{7/2}$ shell model orbital, perturbed into a Nilsson-like state by the rapid onset of deformation. The ground state of ^{141}La is closer to the N=82 major shell closure and is characterized by a single-particle $\pi g_{7/2}$ state. The decay of ^{141}Ba to ^{141}La can be described as the transition $\nu f_{7/2}([532]3/2^{-}) \rightarrow \pi g_{7/2}(7/2^{+})$. As the β decay is between N=5 and N=4 major shells there is an inferred parity change, so the decays fall into the "forbidden" category and have commensurately larger log(ft) values in addition to lack of overlap in the initial and final wave functions.

II. THE EXPERIMENT

An experiment to study the decay of ^{141}Ba into ^{141}La was conducted at Argonne National Laboratory (ANL) using the Gammasphere array [23]. A beam of ^{141}Cs was produced from the CARIBU fission ion source [24] and accelerated through the ATLAS linac to 600 MeV and 850 MeV. The ^{141}Cs beam was implanted into a 50 mg/cm^2 lead foil at the center of Gammasphere where it β decayed into ^{141}Ba ($T_{1/2}$=24.84(17) sec) [25], followed by the β decay of ^{141}Ba into ^{141}La ($T_{1/2}$= 18.27(7) min) [25] and then into ^{141}Ce ($T_{1/2}$ = 3.92(3) hours). For this study the Gammasphere array consisted of 99 Compton-suppressed HPGe detectors. Data were collected with a digital data acquisition system selecting all multiplicity > 1 "singles" triggers for 84.6 hours; 4.9x10^8 single γ-ray events and 1.1x10^8 γ-γ coincident events were collected on disc.

The singles spectrum of the decay chain, ^{141}Cs $\rightarrow$ ^{141}Ba $\rightarrow$ ^{141}La $\rightarrow$ ^{141}Ce is shown in Fig. 1(a). The spectrum is dominated by the lines corresponding to the decay of ^{141}Cs and ^{141}Ba. Despite the complexity of this spectrum, transitions arising from the depopulation of levels in ^{141}La can be easily separated in the γ-γ coincidence matrix as illustrated in Fig. 1(b).

The data were sorted with the GSSort package [26] into singles histograms and $\gamma\gamma$ coincidence matrices. Data analysis was performed with the Radware package [27], gf3m, modified for matrix analysis. Energy calibrations were performed internally using previously well-characterized transitions from the decays of ^{141}Cs and ^{141}Ba and described by a linear function. Those transitions include 555.15 (1)-, 561.63 (1)-, 588.79 (1)-, and 646.66 (1)-keV in the decay of ^{141}Cs [25], 190.328 (5)-, 276.95 (1)-, 304.19 (2)-, 343.67 (2)-, 1501.4-, 1820.5 -, and 2277.9-keV in the decay of ^{141}Ba [25].

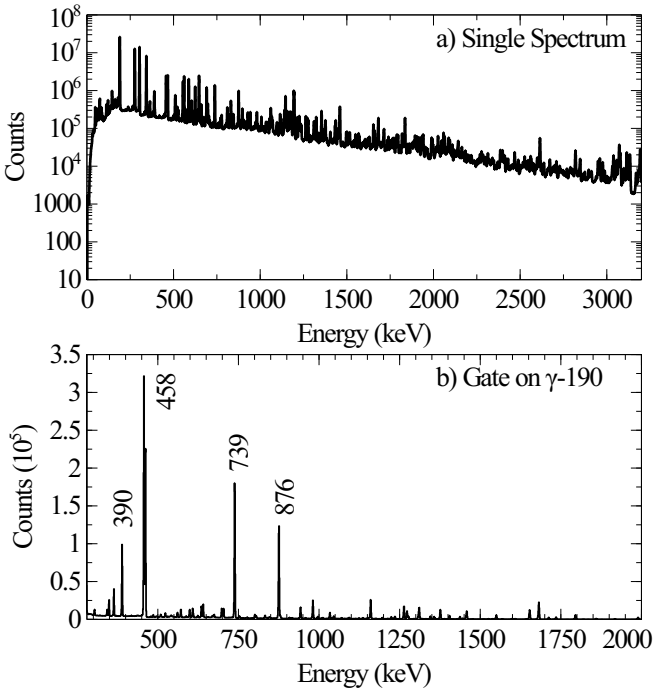

FIG. 1: (a) Singles spectrum from the decay of ^{141}Cs including all subsequent daughters. (b) Background subtracted gate on the 190-keV transition in ^{141}La. Strong transitions in ^{141}La are labeled by their energy in keV.

A 0.2 keV systematic uncertainty was estimated and added in quadrature to the statistical uncertainty in the energy determination. Efficiency calibrations were performed with well-characterized transitions in the decay of ^{152}Eu [28], ^{56}Co [29], and ^{182}Ta [30]. An additional uncertainty of 2% was applied to all measured intensities, to take into account the systematic uncertainty in the efficiency calibration.

The new decay scheme was developed by inspecting the coincidence relationships between γ rays, starting from those already known. Most γ-ray intensities were determined by selecting a transition depopulating a level and determining the area of a transition feeding into that level. The intensity was deduced from the area, corrected for the efficiencies of the gating and measured transitions and the branching ratio of the depopulating transition. The intensities were normalized relative to the strongest transition in the level scheme, taking $I_\gamma(190\gamma)$=1000.

The spins and parities of the levels were assigned from an analysis of γ-γ directional angular correlations for selected pairs of transitions. All pairs of γ-rays ($E_{\gamma 1}$, $E_{\gamma 2}$) within specific range of angles were grouped into ten different angle bins. The normalized intensity distribution with respect to these angles yielded the angular correlation between transitions γ_1 and γ_2.

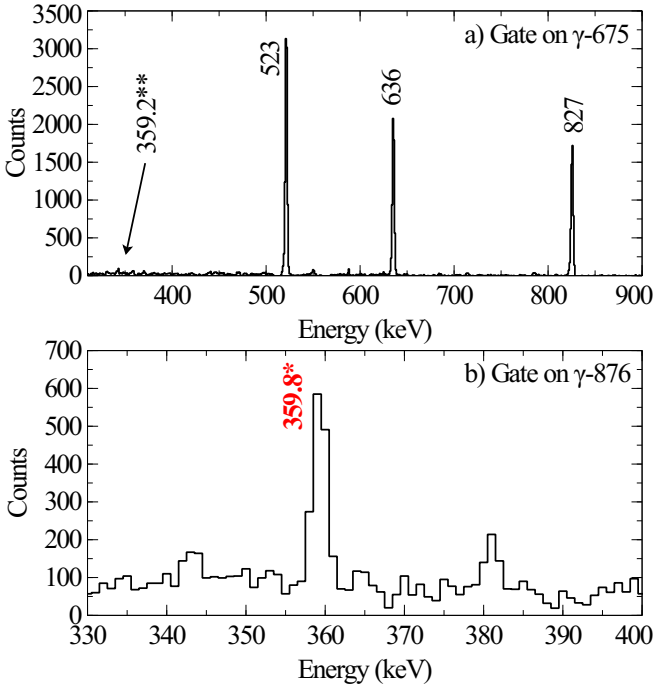

FIG. 2: (Color online) Spectra supporting the new placement of a 359.8-keV transition. (a) Spectrum obtained by gating on the 675-keV transition which feeds into the 826-keV level. The ** on the 359.2-keV transition is to emphasize that the transition is not present or in coincidence with transitions that depopulate the 826-keV energy level. (b) Spectrum obtained by gating on the 876-keV transition which depopulates the level at 1067 keV. The 359.8-keV transition is outlined in red with an * to symbolize the transition being relocated between the 1426- to 1067-keV energy levels.

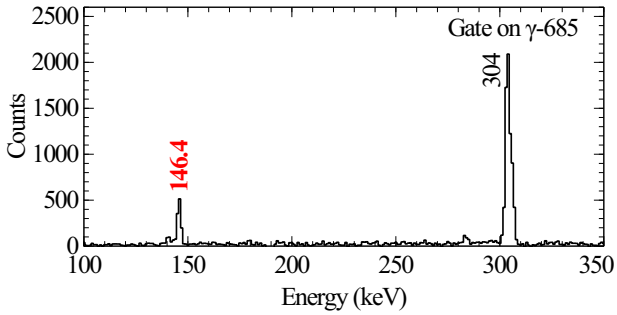

FIG. 3: (Color online) Spectrum providing evidence for a newly observed 146.4-keV transition (in red). Spectrum obtained by gating on the 685-keV ground-state transition. The 304-keV transition observed in this gate results from a 687-keV transition from the 992-keV level, which is not completely resolved from the 685-keV transition, and known to be in coincidence with the 304-keV transition.

III. EXPERIMENTAL RESULTS

Table I lists the energies and intensities of the γ rays assigned to the decay of ^{141}Ba in the present work. The table includes the addition of 8 new levels and the removal of 3, due to lack of evidence. It also includes 60 newly observed transitions, 11 transitions relocated in the level scheme, and 6 transitions now placed in the level scheme which were previously identified as belonging to the decay of ^{141}Ba, but not placed in the decay scheme. The energies of excited states in ^{141}La were derived from a least-squares fit to all measured γ-ray energies. The level scheme drawing is provided as supplemental material [31].

A. Decay Scheme Construction

A level at 826 keV was proposed by Faller *et al.,* [22] on the basis of four depopulating transitions. In the present work, we confirm the strong 523-, 636-, and 827-keV transitions to the 304-, 190-, and 0.0-keV levels, respectively. Faller *et al*., [22] placed an additional weak transition of 359.2 keV as populating the 467-keV level. The present $\gamma\gamma$ coincidence analysis identifies a 359.8(2)-keV transition, however, placed as depopulating the 1426-keV level. Evidence for this new placement is provided in Fig. 2. In Fig. 2(a), a coincidence gate on the 675-keV transition which populates the 826-keV level is presented. The three strong depopulating transitions are clearly observed, while a 359.2-keV transition is absent. In a gate on the 876-keV transition which depopulates the 1067-keV level, clear evidence for a 359.8-keV transition is observed, as shown in Figure 2(b). The observed coincidence relations led to the new placement of the 359.8-keV transition as depopulating the level at 1426 keV. The close agreement between the present measured intensity and that given by Ref. [22] suggests that this is the same transition as reported by Ref. [22].

Faller *et al.,* [22] observed a level at 832 keV based on 364-, 527-, 641-, and 831-keV depopulating transitions which feed into the 467-, 304-, 190-, and 0.0-keV levels, respectively. The present work confirms both the energies and intensities of the above mentioned transitions. Additionally, we observe a weak depopulating transition of 146.4(2) keV feeding into the 685-keV level. Figure 3 provides a gate on the 685-keV ground state transition, with evidence for the newly observed 146.4-keV transition.

The 992-keV level was proposed by Faller *et al.,* [22] on the basis of 687- and 801-keV transitions feeding into the 304- and 190-keV levels, respectively. These transitions were reported with intensities of $I_\gamma(687)=1.1(3)$ and $I_\gamma(801)=2.9(4)$, relative to $I_\gamma(190\gamma)=1000$. In the present work, the two strong depopulating transitions are observed with nearly equal intensities. This is illustrated in Fig. 4 which shows a gate on the 881-keV transition which populates the 992-keV level. Here the 687- and 801-keV transitions are observed with nearly equal intensities (Table I). Additionally, in the present work, we identify two new depopulating transitions at 160.5(2) keV and 165.9(3) keV which are also clearly observed in Fig. 4.

For the higher excited levels, the γ γ coincidence analysis identified alternative placements for a number of transitions, as summarized in Table I. For example, the present work finds no evidence for the proposed 2774.3-, 2441.1-

TABLE I: Levels populated in the ^{141}Ba decay to ^{141}La and their γ-ray decay. The relative intensities for the depopulating γ-ray transitions are given by I_γ. The intensities are normalized to I_γ (190keV)=1000. The intensities are also compared with those from Faller *et al.,* [22]. Energies of excited states were derived from a least-squares fit to all measured γ-ray energies. Multipolarities and mixing ratios are from an angular correlation analysis, see text and Table II and III. Assumed multipolarities are given in square brackets.

J_i^π	E_i (keV)	J_f^π	E_f (keV)	E_γ (keV)	I_γ	Mult.	δ	I_γ^{lit}([22])
$5/2^{(+)}$	190.40(20)	$7/2^{(+)}$	0.00	190.47(20)	1000(20)	$M1(+E2)$	0.007(11)	1000(30)
$5/2^{(+)}$	304.20(8)	$5/2^{(+)}$	190.40	114.10(22)	2.43(5)	$M1+E2$	0.8(2)	2.3(1)
		$7/2^{(+)}$	0.00	304.23(20)	583(11)	$M1+E2$	-0.44(8)	553(17)
$3/2^{(+)}$	467.37(8)	$5/2^{(+)}$	304.20	163.26(20)	9.92(25)	$M1+E2$	0.035(13)	6.4(7)
		$5/2^{(+)}$	190.40	277.01(20)	527(11)	$M1+E2$	0.448(12)	509(15)
		$7/2^{(+)}$	0	467.22(20)	125(3)	$E2$		124(4)
$1/2^{(+)}$	580.17(10)	$3/2^{(+)}$	467.37	113.14(21)	17.4(5)	$M1+E2$	-0.16(11)	22(2)
		$5/2^{(+)}$	190.40	389.74(20)	30.6(7)	$E2$		29(1)
$3/2^{(+)}$	647.94(8)	$1/2^{(+)}$	580.17	67.52(32)	< 0.05			< 0.05
		$3/2^{(+)}$	467.37	180.81(21)	12.2(3)	$M1+E2$	-0.8(6)	11.2(35)
		$5/2^{(+)}$	304.20	343.68(20)	338(7)	$M1+E2$	0.026(2)	314(9)
		$5/2^{(+)}$	190.40	457.51(20)	112(2)	$M1+E2$	0.75(6)	109(3)
		$7/2^{(+)}$	0.00	647.78(21)	127(3)	$E2$		137(4)
$3/2^{(+)}$	685.40(10)	$5/2^{(+)}$	304.20	381.20(21)	3.06(9)	$M1+E2$	-0.21(2)	2.6(4)
		$7/2^{(+)}$	0	685.35(22)	9.52(26)	$[E2]$		4(1)
$5/2^{(+)}$	826.42(10)	$5/2^{(+)}$	304.20	522.74(20)	16.1(4)	$M1+E2$	0.16(3)	9.4(3)
		$5/2^{(+)}$	190.40	635.91(20)	7.0(2)	$M1+E2$	-3.1(16)	6.9(3)
		$7/2^{(+)}$	0.00	826.55(21)	10.8(3)	[M1+E2]		8.6(5)
$3/2^{(+)}$	831.66(8)	$3/2^{(+)}$	685.40	146.4(2)^b	0.40(3)	[M1+E2]		
		$3/2^{(+)}$	467.37	364.32(21)	14.0(3)	$M1+E2$	0.11(9)	12.8(6)
		$5/2^{(+)}$	304.20	527.33(20)	8.2(2)	$M1+E2$	-1.3(2)	9.9(15)
		$5/2^{(+)}$	190.40	641.19(20)	8.23(22)	$M1+E2$	0.08(7)	8.7(4)
		$7/2^{(+)}$	0.00	831.46(20)	36.5(8)	$[E2]$		35.1(17)
$5/2^{(+)}$	929.44(9)	$3/2^{(+)}$	647.94	281.60(21)	2.75(10)	$[M1+E2]$		2.2(3)
		$1/2^{(+)}$	580.17	349.28(20)	7.6(2)	$[E2]$		5.0(4)
		$3/2^{(+)}$	467.37	462.06(20)	113(2)	$M1+E2$	0.025(11)	106(3)
		$5/2^{(+)}$	304.20	625.08(20)	77(2)	$M1+E2$	0.51(1)	78(2)
		$5/2^{(+)}$	190.40	738.95(22)	98(2)	$M1+E2$	0.75(5)	105(3)
		$7/2^{(+)}$	0.00	929.48(24)	16.0(3)	$[M1+E2]$		16.3(9)
$3/2^{(-)}$	991.97(10)	$3/2^{(+)}$	831.66	160.5(2)^b	0.71(4)	$[E1]$		
		$5/2^{(+)}$	826.42	165.9(3)^b	0.55(3)	$[E1]$		
		$5/2^{(+)}$	304.20	687.42(21)	2.66(8)	$E1$		1.1(3)
		$5/2^{(+)}$	190.40	801.47(22)	2.57(9)	$E1$		2.9(4)
$5/2^{(+)}$	1039.48(9)	$5/2^{(+)}$	826.42	213.28(24)^b	0.36(5)	$[M1+E2]$		
		$3/2^{(+)}$	685.40	353.94(24)^b	0.26(2)	$[M1+E2]$		
		$3/2^{(+)}$	467.37	572.10(21)	6.17(17)	$M1(+E2)$	0.01(2)	5.7(5)
		$5/2^{(+)}$	304.20	735.07(21)^b	0.18(2)	$[M1+E2]$		
		$7/2^{(+)}$	0.00	1039.48(23)	1.53(4)	$[M1+E2]$		1.9(3)
$3/2^{(-)}$	1066.57(10)	$3/2^{(+)}$	831.66	235.01(22)	1.08(5)	$[E1]$		1.3(3)
		$3/2^{(+)}$	647.94	418.60(21)	1.39(5)	$[E1]$		1.4(3)
		$1/2^{(+)}$	580.17	486.35(22)	1.60(6)	$[E1]$		1.3(3)
		$3/2^{(+)}$	467.37	599.14(22)	5.98(17)	$[E1]$		5.8(5)
		$5/2^{(+)}$	304.20	762.23(21)	4.38(14)	$E1$		4.2(6)
		$5/2^{(+)}$	190.40	876.09(20)	77(2)	$E1$		80.0(27)

TABLE I: (continued)

J_i^π	E_i (keV)	J_f^π	E_f (keV)	E_γ (keV)	I_γ	Mult.	δ	I_γ^{lit}([22])
$1/2^{(+)}$	1171.99(9)	$5/2^{(+)}$	929.44	242.67(21)	1.72(7)	$[E2]$		2.0(3)
		$3/2^{(+)}$	647.94	523.98(20)	10.1(3)	$M1+E2$	-0.6(2)	10.0(4)
		$3/2^{(+)}$	467.37	704.59(21)	7.34(20)	$M1+E2$	-0.38(2)	5.8(6)
		$5/2^{(+)}$	304.20	867.66(21)	3.19(10)	$E2$		2.4(4)
		$5/2^{(+)}$	190.40	981.52(20)	15.7(5)	$E2$		16(2)
	1188.97(15)	$5/2^{(+)}$	929.44	259.53(20)[b]	0.42(3)			
		$1/2^{(+)}$	580.17	608.71(20)	5.77(17)			8.0(9)
$3/2^{(-)}$	1426.36(10)	$1/2^{(+)}$	1171.99	254.45(20)[d]	0.23(2)	$[E1]$		0.2(1)
		$3/2^{(-)}$	1066.57	359.8(2)[c]	0.28(2)	$[M1+E2]$		0.21(17)
		$5/2^{(+)}$	929.44	496.87(20)[b]	0.73(5)	$[E1]$		
		$3/2^{(+)}$	831.66	594.63(20)[b]	0.76(4)	$[E1]$		
		$3/2^{(+)}$	685.40	741.06(24)[b]	0.36(2)	$[E1]$		
		$3/2^{(+)}$	647.94	778.36(21)	2.43(9)	$[E1]$		1.7(4)
		$1/2^{(+)}$	580.17	846.21(23)	1.4(2)	$[E1]$		1.4(2)
		$3/2^{(+)}$	467.37	959.05(23)[d]	0.89(5)	$[E1]$		1.2(3)
		$5/2^{(+)}$	304.20	1122.13(20)[b]	0.35(3)	$[E1]$		
		$5/2^{(+)}$	190.40	1235.96(20)	2.69(10)	$E1$		4.2(5)
$5/2^{(+)}$	1501.56(9)	$5/2^{(+)}$	1039.48	462.23(22)	0.81(3)	$[M1+E2]$		1.2(6)
		$3/2^{(-)}$	991.97	509.63(20)	1.67(7)	$[E1]$		3(1)
		$3/2^{(+)}$	831.66	669.89(21)	3.46(12)	$[M1+E2]$		4.0(4)
		$5/2^{(+)}$	826.42	675.26(21)	5.5(2)	$[M1+E2]$		6.6(6)
		$3/2^{(+)}$	685.40	815.96(26)[b]	0.21(2)	$[M1+E2]$		
		$3/2^{(+)}$	467.37	1034.24(21)	7.1(2)	$M1+E2$	0.8(5)	4.1(9)
		$5/2^{(+)}$	304.20	1197.28(22)	97(2)	$M1+E2$	-0.24(2)	104(3)
		$5/2^{(+)}$	190.40	1310.73(20)	16.7(4)	$M1+E2$	0.14(6)	14.3(10)
		$7/2^{(+)}$	0.00	1501.79(26)	7.14(18)	$[M1+E2]$		8.5(13)
$1/2^{(+)}$	1547.69(17)[a]	$5/2^{(+)}$	826.42	721.2(3)[b]	0.50(5)	$[E2]$		
		$3/2^{(+)}$	467.37	1080.32(28)[b]	0.24(2)	$[M1+E2]$		
		$5/2^{(+)}$	190.40	1357.33(22)[d]	2.99(11)	$E2$		2.3(3)
	1551.45(14)	$5/2^{(+)}$	190.40	1361.32(20)	0.63(5)			0.70(25)
	1565.98(24)	$3/2^{(+)}$	685.40	880.58(21)	2.36(9)			0.7(4)
	1605.51(16)[a]	$3/2^{(+)}$	831.66	773.83(29)[b]	0.51(4)			
		$3/2^{(+)}$	647.94	957.61(26)[b]	0.31(3)			
		$5/2^{(+)}$	304.20	1301.29(22)[c]	1.69(7)			2.4(3)
$3/2^{(-)}$	1628.16(10)	$1/2^{(+)}$	1171.99	456.48(22)[b]	2.14(9)	$[E1]$		
		$3/2^{(-)}$	1066.57	561.48(21)	2.76(9)	M1+E2	-0.8(5)	4.1(5)
		$5/2^{(+)}$	1039.48	588.81(22)	0.78(4)	$[E1]$		2.7(4)
		$5/2^{(+)}$	929.44	698.61(21)	9.3(3)	$E1$		8.7(5)
		$3/2^{(+)}$	831.66	796.36(25)[b]	0.65(4)	$[E1]$		
		$3/2^{(+)}$	647.94	980.16(22)	1.64(7)	$[E1]$		4(1)
		$3/2^{(+)}$	467.37	1160.72(21)	25.1(6)	$E1$		24(1)
		$5/2^{(+)}$	304.20	1323.92(20)	20.6(5)	$E1$		21(1)
		$5/2^{(+)}$	190.40	1437.75(21)	2.90(10)	$E1$		4.2(8)
	1716.50(14)	$3/2^{(+)}$	831.66	884.83(20)	1.08(6)			1.0(2)
		$1/2^{(+)}$	580.17	1136.24(24)	0.92(5)			0.8(2)
		$5/2^{(+)}$	190.40	1526.14(20)[d]	0.40(3)			1.1(3)

TABLE I: (continued)

J_i^π	E_i (keV)	J_f^π	E_f (keV)	E_γ (keV)	I_γ	Mult.	δ	I_γ^{lit}([22])
$5/2^{(+)}$	1740.69(10)	$3/2^{(-)}$	991.97	748.72(20)[b]	0.48(3)	$[E1]$		
		$3/2^{(+)}$	831.66	909.01(21)	2.56(10)	$[M1+E2]$		2.5(4)
		$3/2^{(+)}$	685.40	1055.23(23)	1.18(6)	$[M1+E2]$		2.0(4)
		$3/2^{(+)}$	647.94	1092.76(22)	1.57(7)	$[M1+E2]$		2(1)
		$3/2^{(+)}$	467.37	1273.43(21)	11.1(3)	$M1(+E2)$	0.02(2)	10.9(7)
		$5/2^{(+)}$	304.20	1436.47(20)	14.5(3)	$M1+E2$	-0.24(6)	18.8(12)
		$5/2^{(+)}$	190.40	1550.45(21)	5.75(18)	$M1+E2$	-1.3(5)	8.5(5)
		$7/2^{(+)}$	0.00	1740.67(20)[d]	6.19(17)	$[M1+E2]$		7.1(6)
$3/2^{(-)}$	1844.30(11)		1188.97	655.21(23)[d]	0.36(2)			0.4(3)
		$5/2^{(+)}$	1039.48	804.60(22)	0.99(8)	$[E1]$		1.4(3)
		$3/2^{(+)}$	831.66	1012.48(21)	2.68(11)	$[E1]$		3.2(5)
		$1/2^{(+)}$	580.17	1264.69(20)	17.1(4)	$[E1]$		19(1)
		$3/2^{(+)}$	467.37	1376.86(21)	15.4(4)	$[E1]$		18(1)
		$5/2^{(+)}$	304.20	1539.80(23)	0.94(4)	$[E1]$		1.8(2)
		$5/2^{(+)}$	190.40	1653.83(20)	14.2(3)	$E1$		20(1)
$1/2^{(+)}$	1872.60(9)		1551.45	321.39(20)	0.20(1)			0.6(3)
		$1/2^{(+)}$	1171.99	700.50(22)	2.42(10)	$[M1]$		2.8(3)
		$3/2^{(-)}$	1066.57	805.91(21)	1.69(7)	$[E1]$		1.4(3)
		$5/2^{(+)}$	1039.48	833.06(21)	3.17(5)	$[E2]$		3.6(8)
		$3/2^{(-)}$	991.97	880.63(21)	3.80(15)	$[E1]$		3.2(5)
		$5/2^{(+)}$	929.44	943.07(20)	16.7(5)	$[E2]$		17.5(9)
		$5/2^{(+)}$	826.42	1046.18(21)	7.0(3)	$[E2]$		7.4(9)
		$3/2^{(+)}$	685.40	1187.35(26)	0.38(3)	$[M1+E2]$		0.24(19)
		$3/2^{(+)}$	647.94	1224.60(20)	8.8(2)	$[M1+E2]$		9.5(13)
		$3/2^{(+)}$	467.37	1405.25(20)	5.65(17)	$M1+E2$	-0.25(2)	7.1(5)
		$5/2^{(+)}$	304.20	1568.41(21)	4.67(14)	$E2$		6.1(6)
		$5/2^{(+)}$	190.40	1682.19(20)	26.5(7)	$E2$		37(2)
$3/2^{(-)}$	1926.01(10)	$1/2^{(+)}$	1171.99	753.87(22)	1.79(8)	$[E1]$		1.0(4)
		$5/2^{(+)}$	929.44	996.51(22)	2.92(13)	$[E1]$		2.8(5)
		$3/2^{(+)}$	831.66	1094.36(21)	3.62(14)	$[E1]$		3(1)
		$3/2^{(+)}$	647.94	1277.98(20)	14.1(3)	$E1$		14.4(8)
		$1/2^{(+)}$	580.17	1345.83(21)	3.54(13)	$[E1]$		3.9(4)
		$3/2^{(+)}$	467.37	1458.48(21)	14.0(4)	$E1$		16.6(15)
		$5/2^{(+)}$	304.20	1621.74(22)	1.25(5)	$[E1]$		1.5(4)
		$5/2^{(+)}$	190.40	1735.69(21)[d]	3.41(12)	$E1$		4.6(8)
$3/2^{(-)}$	2180.38(12)	$1/2^{(+)}$	1171.99	1008.45(24)[d]	0.93(6)	$[E1]$		1.4(3)
		$3/2^{(+)}$	647.94	1532.45(25)[b]	0.51(3)	$[E1]$		
		$1/2^{(+)}$	580.17	1600.19(24)	1.13(6)	$[E1]$		1.4(3)
		$3/2^{(+)}$	467.37	1712.98(21)[c]	3.89(12)	$E1$		4.6(8)
		$5/2^{(+)}$	304.20	1876.12(24)[b]	0.60(5)	$[E1]$		
		$5/2^{(+)}$	190.40	1989.97(21)[c]	3.79(12)	$E1$		5.4(10)
$1/2^{(+)}$	2216.56(11)	$5/2^{(+)}$	1039.48	1176.91(20)	0.77(2)	$[E2]$		1.5(3)
		$3/2^{(+)}$	831.66	1385.03(25)[b]	0.44(3)	$[M1+E2]$		
		$5/2^{(+)}$	826.42	1390.35(26)	1.14(10)	$[E2]$		1.2(3)
		$3/2^{(+)}$	647.94	1568.7(2)	1.42(6)	$[M1+E2]$		6.1(6)
		$3/2^{(+)}$	467.37	1748.73(22)[b]	0.12(2)	$[M1+E2]$		
		$5/2^{(+)}$	304.20	1912.40(21)[c]	2.99(10)	$E2$		3.3(5)
		$5/2^{(+)}$	190.40	2026.38(21)[d]	8.02(23)	$E2$		9.8(15)

TABLE I: (continued)

J_i^π	E_i (keV)	J_f^π	E_f (keV)	E_γ (keV)	I_γ	Mult.	δ	I_γ^{lit} ([22])
$3/2^{(-)}$	2327.22(14)[a]	$1/2^{(+)}$	1171.99	1155.07(20)[b]	0.57(4)	$[E1]$		
		$3/2^{(+)}$	831.66	1494.95(32)[b]	0.17(3)	$[E1]$		
		$3/2^{(+)}$	647.94	1679.28(24)[b]	0.69(4)	$[E1]$		
		$3/2^{(+)}$	467.37	1859.89(22)[d]	1.66(7)	$[E1]$		2.0(3)
		$5/2^{(+)}$	304.20	2023.39(22)[b]	0.06(1)	$[E1]$		
		$5/2^{(+)}$	190.40	2136.81(20)[d]	1.81(7)	$E1$		0.7(2)
	2345.2(3)[a]	$5/2^{(+)}$	304.20	2041.03(27)[b]	0.22(1)			
$3/2^{(-)}$	2375.85(12)	$3/2^{(-)}$	1926.01	449.7(2)[b]	0.47(4)	$[M1+E2]$		
		$3/2^{(-)}$	1066.57	1309.23(21)	4.07(14)	$M1+E2$	0.6(3)	5.1(7)
		$5/2^{(+)}$	929.44	1446.48(20)	1.65(9)	$[E1]$		3.1(4)
		$3/2^{(+)}$	647.94	1727.99(20)[d]	1.52(7)	$[E1]$		2.0(2)
		$1/2^{(+)}$	580.17	1795.71(21)[d]	8.26(26)	$[E1]$		12.5(9)
$3/2^{(-)}$	2385.68(11)	$1/2^{(+)}$	1171.99	1213.57(20)[b]	0.50(4)	$[E1]$		
		$5/2^{(+)}$	929.44	1456.21(20)	2.15(11)	$[E1]$		2.8(7)
		$1/2^{(+)}$	580.17	1805.48(37)[b]	0.06(1)	$[E1]$		
		$3/2^{(+)}$	467.37	1918.38(20)[c]	1.07(5)	$[E1]$		1.3(2)
		$5/2^{(+)}$	304.20	2081.35(22)[b]	0.37(3)	$[E1]$		
		$5/2^{(+)}$	190.40	2195.4(2)[d]	1.79(7)	$E1$		2.1(3)
$5/2^{(+)}$	2468.74(9)	$3/2^{(-)}$	1926.01	542.5(2)	0.95(6)	$[E1]$		1.8(5)
		$3/2^{(-)}$	1628.16	840.5(2)	1.09(4)	$[E1]$		1.0(2)
			1551.45	917.32(20)	0.56(3)			1.2(2)
		$5/2^{(+)}$	1501.56	967.05(20)	0.54(3)	$[M1+E2]$		0.7(2)
		$1/2^{(+)}$	1171.99	1296.72(21)[b]	0.27(3)	$[E2]$		
		$3/2^{(-)}$	991.97	1476.62(21)[b]	0.25(3)	$[E1]$		
		$5/2^{(+)}$	929.44	1539.40(20)	0.79(6)	$[M1+E2]$		1.8(2)
		$5/2^{(+)}$	826.42	1642.39(25)	1.16(8)	$[M1+E2]$		1.8(3)
		$3/2^{(+)}$	647.94	1820.86(20)	1.68(7)	$[M1+E2]$		2.6(3)
		$3/2^{(+)}$	467.37	2001.8(5)[b]	0.06(1)	$[M1+E2]$		
		$5/2^{(+)}$	304.20	2164.51(21)[c]	3.66(12)	$M1+E2$	-0.34(18)	3.9(9)
		$5/2^{(+)}$	190.40	2278.46(20)	1.88(7)	$[M1+E2]$		2.4(2)
		$7/2^{(+)}$	0.00	2468.86(21)	4.44(11)	$[M1+E2]$		5.3(3)
	2485.8(4)[a]	$3/2^{(+)}$	831.66	1654.21(38)[b]	0.14(2)			
		$5/2^{(+)}$	304.20	2181.32(36)[b]	0.03(1)			
	2700.36(14)[a]	$5/2^{(+)}$	929.44	1770.77(36)[b]	0.21(3)			
		$3/2^{(+)}$	831.66	1868.38(33)[b]	0.15(2)			
		$3/2^{(+)}$	647.94	2052.14(39)[b]	0.14(1)			
		$1/2^{(+)}$	580.17	2120.04(29)[b]	0.28(2)			
		$5/2^{(+)}$	304.20	2396.68(22)[b]	0.04(1)			
		$5/2^{(+)}$	190.40	2509.49(35)[b]	0.12(1)			
	2772.45(17)[a]	$3/2^{(+)}$	647.94	2124.4(4)[b]	0.09(1)			
		$3/2^{(+)}$	467.37	2304.41(27)[b]	0.38(3)			
		$5/2^{(+)}$	304.20	2468.68(22)[b]	0.04(1)			
	2808.5(3)[a]	$3/2^{(+)}$	647.94	2160.9(4)[b]	0.06(1)			
		$1/2^{(+)}$	580.17	2228.04(32)[b]	0.12(2)			

TABLE I: (continued)

J_i^π	E_i (keV)	J_f^π	E_f (keV)	E_γ (keV)	I_γ	Mult.	δ	I_γ^{lit}([22])
	2956.0(3)[a]	$3/2^{(+)}$	647.94	2308.02(45)[b]	0.03(1)			
		$5/2^{(+)}$	304.20	2651.7(5)[b]	0.03(1)			
		$5/2^{(+)}$	190.40	2765.6(5)[b]	0.02(1)			

[a]Newly observed energy level.
[b]Newly observed γ-ray transition.
[c]Relocated γ-ray transition from the evaluated level scheme.
[d]γ-ray transition previously observed, but unplaced in the decay of ^{141}Ba.

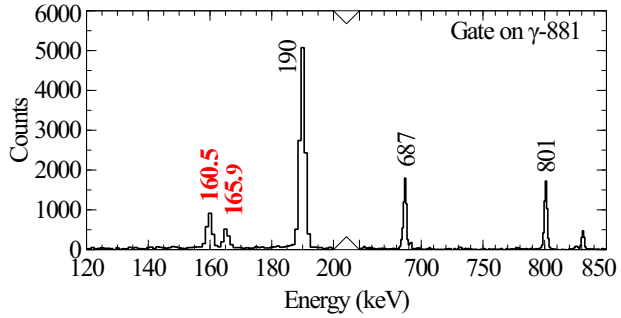

FIG. 4: (Color online) Spectrum providing support for newly identified 160.5- and 165.9-keV transitions (in red) depopulating the level at 992 keV. Spectrum was obtained by gating on the 881-keV transition which feeds into the 992-keV level. Note the break in the x axis energy between 200 and 650 keV.

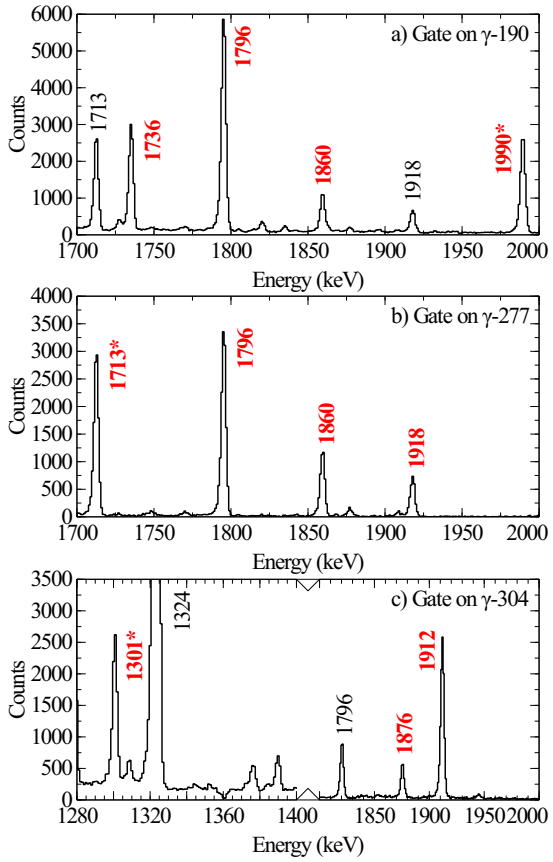

FIG. 5: (Color online) Spectra gated on the a) 190-keV, b) 277-keV and c) 304-keV transitions, providing evidence of new transitions (in red) and evidence to remove the 2293.7-keV energy level by relocating it's depopulating transitions (in red with an *). Note the cut in the x axis energy in panel (c).

and 2293.7-keV levels [22] after relocating the transitions that depopulate those levels. Evidence to remove the previously proposed 2293.7-keV level by relocating the 1301.29(22)-, 1712.98(21)- and 1989.97(21)-keV depopulating transitions (reported as 1302.1, 1712.7, and 1990.0 respectively in Ref. [22]) is given in Fig. 5. The 1990-keV transition was previously suggested to depopulate the 2293.7-keV level and feed into the 304-keV level. Figure 5(c) provides a gate on the 304-keV transition where no coincidence with a 1990-keV transition is observed. In contrast, Fig. 5(a) shows a gate on the 190-keV transition where coincidence with a 1990-keV transition is clearly observed. Both the $\gamma\,\gamma$ coincidence relationships and energy sums, suggest that the 1990-keV transition depopulates a previously observed level at 2180 keV. A 1713-keV transition was previously placed [22] as depopulating the 2293.7-keV level and feeding into the 580-keV level. In the present work, we find no coincidence relationship between a 1713-keV transition and the 113- or 390-keV transitions known to depopulate the 580-keV level. Instead, a 1713-keV transition is strongly observed in a gate on the 277-keV transition, as demonstrated in Fig. 5(b), also placing the 1713-keV transition as depopulating the known 2180-keV level. The final transition which formed support for the proposed 2293.7-keV level was a 1302.1-keV transition [22] placed as feeding into the 992-keV level. No evidence was observed for a 1302.1-keV transition in coincidence with either the 687- or 801-keV transitions which depopulate the 992-keV level. As shown in Fig. 5(c), a 1301-keV transition is observed in coincidence with the 304-keV transition. This suggests that the 1301-keV transition depopulates a newly observed level at 1605.5 keV; this is further supported by the observation of two additional depopulating transitions (see Table I).

B. Spin and Parity Assignments

In the evaluated data [25], the ground state spin of ^{141}La is tentative, (7/2$^+$). There is sufficient evidence from the A=141 chain that J=7/2 can be firmly assigned, which is essential for fixing the excited state spins. Both the parent and daughter of ^{141}La have directly measured ground-state spins, with J= 7/2 for ^{141}Ce from paramagnetic resonance [32] and J= 3/2 for ^{141}Ba [33] from hyperfine spectroscopy measurements. ^{141}La decays to 7/2$^-$ and 9/2$^-$ levels in ^{141}Ce with log *ft* values [25] of 7.3 and 7.8, respectively, which limits the J of the ^{141}La ground state to 7/2 or 9/2. Strong β feeding to the 190-keV level from the decay of the J$^\pi$= 3/2$^-$ ground state of ^{141}Ba, limits the J of the 190-keV level to 1/2, 3/2, or 5/2. These spin possibilities, coupled with the known M1 character [25] of the 190-keV γ ray, give J=7/2 for the ground state and J=5/2 for the 190-keV level in ^{141}La. There is no direct experimental evidence for the parity of the ^{141}La ground state. The neighboring nuclei, ^{139}La and ^{137}La, both have J$^\pi$= 7/2$^+$, suggesting positive parity from a systematics argument. Assignment of a single-particle $\pi g_{7/2}$ configuration to the ground state further supports the positive parity assignment. Given that the parity assignment can only be based on systematics and theory considerations, for the subsequent discussion we adopt J$^\pi$=7/2$^{(+)}$ for the ^{141}La ground state.

For a cascade of two $E2/M1$ mixed transitions, the angular correlation can vary considerably depending on the mixing ratio of each transition. Therefore, it is critical to determine the mixing ratio for at least one of the two transitions in the cascade to avoid ambiguity in the spin and multipolarity assignments. In previous studies [19, 21, 22], the 190-keV γ ray was reported as $M1/E2$ in character with the mixing ratio, δ, nearly equal to zero. From conversion electron measurements of α(K) and K/L subshell ratios, the mixing ratio of the 190-keV transition could be constrained to <0.3, with pure M1 being adopted by the evaluated data [25]. This constrains the 190-keV γ as a 5/2$^{(+)}$ to 7/2$^{(+)}$ transition, also based on arguments discussed above. The second excited level populated in ^{141}Ba decay at 304 keV, decays by a 304-keV transition with a measured α(K) of 0.035(5) [25], which indicates mixed multipolarity; theoretical values [34] are 0.044 for an M1 transition and 0.036 for an E2 transition.

As many transitions feed into the 190- and 304-keV levels, it is important to confirm and perhaps better constrain their multipolarities. This was accomplished by first identifying transitions higher in the level scheme with stretched quadrupole or dipole character. In Table I, one finds a subset of levels at 992, 1067, 1172, 1426, 1548, 1628, 1717, 1844, 1873, 1926, 2180, 2217, 2327 and 2386 keV which favorably decay to the 5/2$^{(+)}$ and 3/2$^{(+)}$ states but no transitions to the 7/2$^{(+)}$ ground state are observed. This decay pattern would suggest possible spins and parities for these states of 3/2$^{(-)}$ or 1/2$^{(+)}$ because $M2$ or $M3$ transitions are hindered in the electromagnetic decay of nuclear states when competing with $E1$, $M1$ and $E2$ transitions. As these levels generally have multiple decay paths, different cascades from the same level can be analyzed to determine a consistent J for the initial level in the cascade. Examples of this analysis are given in Figs. 6 and 7, where the measured angular-correlation patterns for pairs of transitions forming cascades with the 190- or 304-keV γ rays agree well with (1/2$^{(+)}$, 3/2$^{(-)}$) $\rightarrow$ 5/2$^{(+)}$ $\rightarrow$ 7/2$^{(+)}$ cascades. With the spin fixed and considering these are stretched quadrupole (for 1/2$^{(+)}$ states) or pure dipole (for 3/2$^{(-)}$ states), the mixing ratio of the 190- and 304-keV transitions can be determined for a number of cascades. These data are provided in Table II. From this analysis, the average $E2/M1$ mixing ratios for the 190- and 304-keV transitions are estimated as $\delta = 0.007(11)$ and $\delta = -0.44(8)$, respectively, which are consistent with those deduced from conversion coefficient measurements [19, 21].

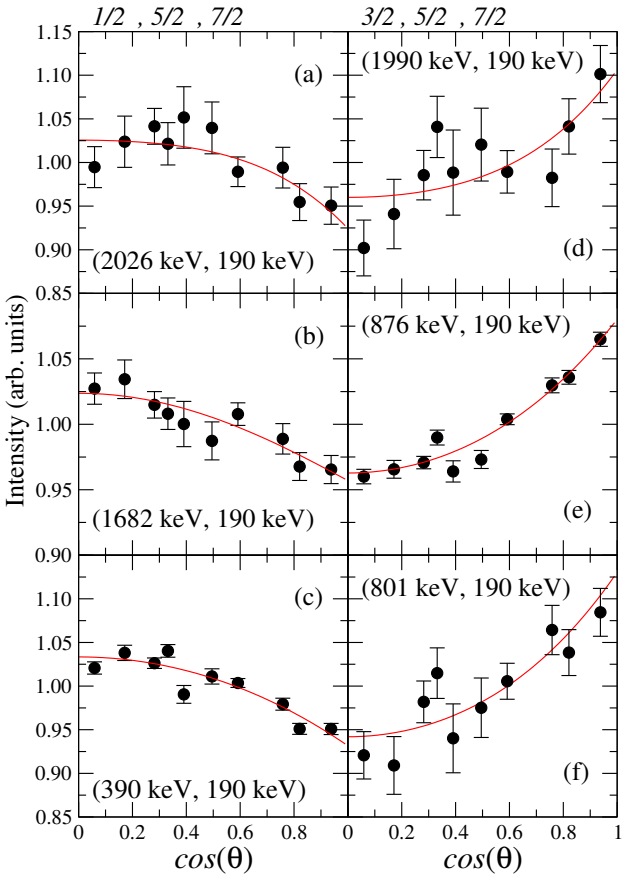

FIG. 6: (Color online) Measured angular correlations for cascades with the 190-keV γ ray as one of the transitions, and the other one decaying from 1/2$^{(+)}$levels, as shown in panels (a), (b) and (c), or from 3/2$^{(-)}$levels, as shown in panels (d),(e), and (f). Red lines in the figures correspond to fitted angular correlation functions with the other γ rays being stretched D or Q transitions.

For the analysis of angular correlations related to $\gamma_1(D/Q) \rightarrow \gamma_2(D/Q)$ cascades with γ_2 as the 190- or 304-keV transition, the mixing ratios in the subsequent analysis are fixed as 0.0 and -0.4, respectively. Then, as demonstrated in Fig. 8, the J and mixing ratio for the first γ ray in the cas-

TABLE II: Results of $\gamma\gamma$ angular correlations used to determine the mixing ratios of 190- and 304-keV transitions. E_i gives the initial level energy, $\gamma_1\gamma_2$ gives the two gamma rays analyzed in the cascade and a_2,a_4 are the coefficients obtained from a fit to Legendre polynomials of the angular correlation data. The assumed multipolarity of the first γ ray in the cascade is given in the $\text{Mult.}_{\gamma 1}$ column and the $\delta_{\gamma 2}$ is the mixing ratio extracted for the 190 or 304 γ ray.

E_i	$\gamma_1\gamma_2$[keV]	a_2	a_4	$\text{Mult.}_{\gamma 1}$	$\delta_{\gamma 2}$
580.17	390-190	-0.067(5)	-0.001(7)	*Q*	-0.006(8)
991.97	801-190	0.11(2)	-0.02(3)	*D*	0.12(4)
991.97	687-304	-0.268(19)	-0.00(3)	*D*	-0.9(1)
1066.57	876-190	0.077(4)	0.003(6)	*D*	0.052(8)
1066.57	762-304	-0.074(18)	0.036(25)	*D*	-0.27(5)
1171.99	982-190	-0.044(9)	0.007(13)	*Q*	-0.037(12)
1171.99	868-304	0.238(19)	-0.01(3)	*Q*	-0.6(2)
1426.36	1236-190	0.07(4)	0.04(5)	*D*	0.04(8)
1547.69	1357-190	-0.07(4)	0.03(6)	*Q*	0.0(5)
1628.16	1438-190	0.05(3)	-0.00(4)	*D*	0.00(5)
1628.16	1324-304	-0.166(8)	-0.014(12)	*D*	-0.6(1)
1844.30	1654-190	0.065(12)	0.020(17)	*D*	0.029(23)
1872.60	1682-190	-0.045(8)	0.002(12)	*Q*	-0.036(11)
1872.60	1568-304	0.187(19)	0.04(3)	*Q*	-0.44(5)
1926.01	1736-190	0.049(24)	-0.08(3)	*D*	0.0(5)
1926.01	1278-344	-0.016(13)	0.007(19)	*D*	0.05(3)
2180.38	1990-190	0.09(2)	0.02(3)	*D*	0.08(4)
2216.56	2026-190	-0.062(17)	-0.014(24)	*Q*	-0.013(23)
2216.56	1912-304	0.18(3)	0.00(4)	*Q*	-0.4(1)
2327.22	2137-190	0.05(4)	0.10(5)	*D*	0.00(8)
2385.68	2195-190	0.13(4)	0.02(5)	*D*	0.15(8)

cade can be determined. The results of the angular correlation analysis for transitions feeding into the 190-, 304-, 467- and 1067-keV levels are summarized in Table III. We apply two assumptions to arrive at the multipolarities given in Table I, first that Q transitions are E2 in character and second, that D+Q transitions with a non-zero mixing ratio are M1+E2 in character. These are both supported by the prompt nature of the transitions observed in coincidence which makes M2 character for the transitions unlikely. In arriving at the J^π assignments given in Table I, we additionally consider the populating and depopulating patterns of the state of interest.

C. Gamma Intensity Normalization

The current evaluated data [25] gives an absolute intensity for the 190.5-keV transition as 45.5(14) %. This is indirectly determined from Ref. [21], where the authors indicate they determined the absolute intensity of the 190.5-keV transition based on the 1354.52-keV absolute intensity in the decay of ^{141}La. Ref. [21], however, does not explicitly provide the absolute intensity, only the ground-state to ground-state β feeding calculated using their decay scheme, which the evaluated data uses to deduce the 190.5-keV transition absolute intensity.

In the present work, we determine the absolute intensity of the 190-keV transition by linking it to the decay of the ^{141}La daughter, taking $I_\gamma(1354\gamma)$=1.64(7)% from Ref. [35]. The decay of ^{141}Cs and subsequent daughter have relatively short half-lives compared to the decay of ^{141}La ($T_{1/2}$= 3.92 (3) hrs), therefore, it would take at least 20 hours for the decay of ^{141}Ba and ^{141}La to reach equilibrium. The full time span of the experiment with beam intensity being stable lasted for 34 hours. The data from the last 3 hours allows us to ensure that an equilibrium condition was met, while obtaining sufficient statistics for the analysis. From the ratio of the 190- and 1354-keV γ-ray intensities, we obtain $I_\gamma(190\gamma)$=44.8(21)%, in excellent agreement with the evaluated data. Note that the uncertainty from our measurement is dominated by that of the intensity of the 1354-keV transition ($\sigma = 4.2\%$), with the combined uncertainty of statistical and detector efficiency in the present work being 2.1%. Because the evaluated $I_\gamma(190\gamma)$ was deduced in a similar manner relying on the independently measured $I_\gamma(1354\gamma)$ value, it is difficult to understand how the evaluated $I_\gamma(190\gamma)$ value achieved a smaller uncertainty than that of $I_\gamma(1354\gamma)$.

IV. DISCUSSION

In the past, comparisons have been made between gamma-ray calorimetry (TAGS) measurements and HPGe spectroscopy, for example in Ref. [6]. There is no doubt that when the decay Q-value is large, 10 MeV or more, fragmentation of the gamma decay paths, "Pandemonium", makes it impossible for even modern large HPGe arrays to track all the decay

TABLE III: Assigned multipolarities and deduced mixing ratios from the $\gamma\gamma$ angular correlation analysis. E_i gives the initial level energy, $\gamma_1\gamma_2$ gives the two gamma rays analyzed in the cascade and a_2,a_4 are the coefficients obtained from a fit to Legendre polynomials of the angular correlation data. Mult.$_{\gamma 1}$ and $\delta_{\gamma 1}$ are the multipolarity and mixing ratio, respectively, determined for the first transition in the cascade. The mixing ratios of the 190- and 304-keV transition are fixed as 0.0 and -0.4, respectively.

E_i	$\gamma_1\gamma_2$[keV]	a_2	a_4	Mult.$_{\gamma 1}$	$\delta_{\gamma 1}$
304.20	114-190	0.04(1)	-0.007(14)	$D+Q$	0.8(2)
467.37	277-190	0.132(1)	-0.0020(17)	$D+Q$	0.448(12)
467.37	163-304	-0.140(8)	0.011(12)	$D+Q$	0.035(13)
580.17	113-467[a]	-0.03(3)	-0.03(3)	$D+Q$	-0.16(11)
647.94	458-190	0.166(4)	-0.003(5)	$D+Q$	0.75(6)
647.94	344-304	-0.135(1)	-0.0008(20)	$D+Q$	0.026(2)
647.94	181-467[a]	0.15(3)	0.06(4)	$D+Q$	-0.8(6)
685.40	381-304	-0.045(15)	-0.074(22)	$D+Q$	-0.21(2)
826.42	636-190	-0.022(16)	-0.017(24)	$D+Q$	-3.1(16)
826.42	523-304	0.081(10)	0.030(15)	$D+Q$	0.16(3)
831.66	641-190	0.069(16)	0.019(23)	$D+Q$	0.08(7)
831.66	527-304	0.335(13)	0.003(18)	$D+Q$	-1.3(2)
831.66	364-467[a]	0.032(20)	0.04(3)	$D+Q$	0.11(9)
929.44	739-190	0.038(3)	0.004(5)	$D+Q$	0.75(5)
929.44	625-304	-0.034(3)	0.010(5)	$D+Q$	0.51(1)
929.44	462-277[b]	0.009(4)	-0.001(6)	$D+Q$	0.025(11)
1039.48	572-277[b]	0.049(13)	0.007(19)	D	0.01(2)
1039.48	572-467[a]	0.02(4)	-0.07(6)	$D(+Q)$	0.2(2)
1171.99	705-277[b]	-0.117(16)	0.008(24)	$D+Q$	-0.38(2)
1171.99	524-647[a]	0.07(3)	0.03(5)	$D+Q$	-0.6(2)
1501.56	1311-190	-0.037(10)	0.017(15)	$D+Q$	0.14(6)
1501.56	1197-304	0.198(4)	0.000(5)	$D+Q$	-0.24(2)
1501.56	1034-467[a]	0.09(4)	0.000(5)	$D+Q$	0.8(5)
1628.16	561-876[c]	-0.12(3)	-0.06(5)	$D+Q$	-0.8(5)
1628.16	1161-467[a]	0.05(2)	-0.02(3)	$D(+Q)$	0.03(9)
1740.69	1550-190	-0.069(18)	0.012(25)	$D+Q$	-1.3(5)
1740.69	1436-304	0.199(10)	0.005(15)	$D+Q$	-0.24(6)
1740.69	1273-277[b]	0.045(13)	-0.026(18)	$D(+Q)$	0.02(2)
1872.60	1405-277[b]	0.023(18)	-0.02(3)	$D+Q$	-0.25(2)
2375.85	1309-876[c]	0.04(3)	0.05(5)	$D+Q$	0.6(3)
2468.74	2165-304	0.214(24)	-0.01(3)	$D+Q$	-0.34(18)

[a] Stretched Q transition used for γ_2 in the angular correlation analysis.
[b] D+Q transition with δ=0.44 used for γ_2 in the angular correlation analysis.
[c] Stretched D transition used for γ_2 in the angular correlation analysis.

strength, and trace the flux from high-lying states. Thus, it has been argued that the TAGS measurements always have the advantage in describing the global features associated with the β-decay strength function, while discrete γ-ray spectroscopy is advantageous for studying individual states fed in β decay. In this specific case, with a more modest Q-value window, the discrete line spectroscopy appears to fully capture all the strength function features extracted from TAGS and, in addition, provides a wealth of new spectroscopic detail. Overall, the more detailed the discrete decay scheme is, the more reliable the additional information that can be extracted from low-resolution TAGS measurements becomes.

A. Gamma-ray Transitions

In the present measurement, γ-ray transitions in the decay of ^{141}Ba have been identified down to the level of 0.002 % of the strongest, 190.5-keV transition, revealing the existence of more weakly populated states. Additionally, the absolute intensity of the 190.5-keV transition has been determined using the absolute intensity of the 1354.5-keV transition in the decay of the daughter nucleus, ^{141}La. Spins and parities are proposed for the majority of states based on the angular correlation measurements, with the determination of multipolarity and mixing ratios for most of the transitions.

The transition intensities are in close agreement when comparing the results of the present work and with those of the

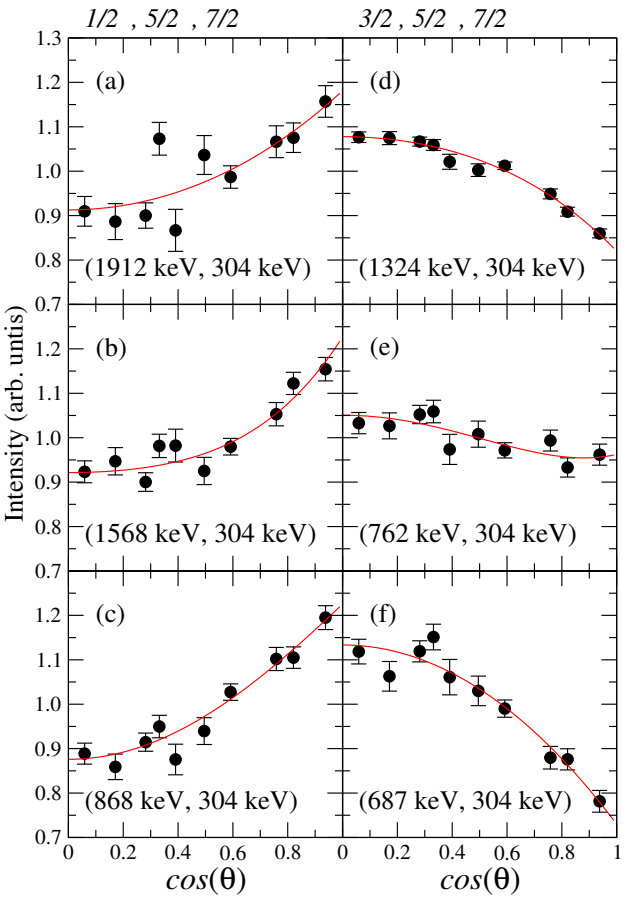

FIG. 7: (Color online) Measured angular correlations for cascades with the 304-keV γ ray as one of the transitions, and the other one decaying from $1/2^+$ levels, as shown in panels (a), (b) and (c), or from $3/2^-$ levels, as shown in panels (d),(e), and (f). Red lines in the figures correspond to fitted angular correlation functions with the other γ rays being stretched D (right panels) or Q (left panels) transitions.

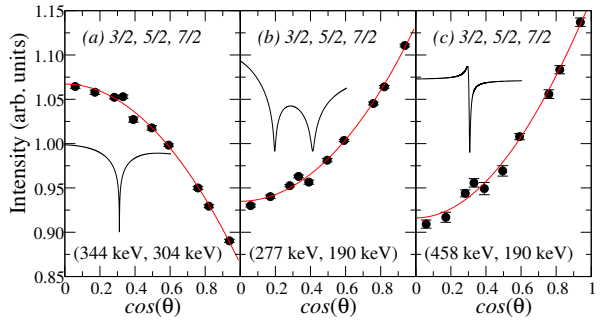

FIG. 8: (Color online) Measured angular correlations for cascades of two $E2/M1$ mixed transitions. Red lines in the figures correspond to fitted angular correlation function with $\delta = -0.4$ for the 304-keV γ ray and $\delta = 0.0$ for the 190-keV γ ray. The mixing ratios δ are determined from minimizing the χ^2 value between theoretical and experimental a_2 and a_4 coefficients as function of mixing ratio. The general feature of χ^2 *vs* δ is demonstrated in the insets.

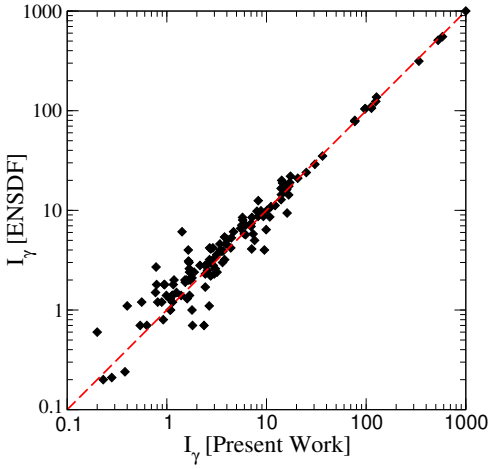

FIG. 9: (Color online) Comparison of discrete γ-ray intensities from the present work to those from the evaluated data [25]. Equal values from both data sets are represented by the red dashed line.

evaluated data [25], as demonstrated in Fig. 9, with a tendency of the higher the intensity the better the agreement. The high-sensitivity of the Gammasphere data can be demonstrated by the observation of a number of new transitions with intensities up to 5 orders of magnitude lower than that of the strongest transition, particularly for high-energy γ rays above 1500 keV.

B. Beta Feeding

The direct β-feeding intensities to each excited level are deduced from the γ-ray intensity imbalance of transitions populating and depopulating each level, with conversion electron contributions taken into account. The code BrIcc [34] was used to calculate conversion coefficients. For transitions with undetermined multipolarities, their conversion coefficients are the average of the theoretical values for dipole or $E2$ multipolarity, with an uncertainty covering the full range. The deduced β feedings are presented in Table IV along with those from the previous evaluated data [25] and from Greenwood *et al.*, [9].

As seen in Fig. 10(a), the β-feeding strength does not exhibit any regularity with respect to excitation energy, a behavior expected in the β-decay process which is governed by two factors: β-decay selection rules and available phase space. The sensitivities of different measurements in determining the β feeding are compared with each other following a practice similar to that presented for the γ intensity comparisons. At first glance, the data points plotted in Fig. 10(b) show no notable deviations from the blue dashed line, which represents the case where the compared datasets have the same values, particularly for $I_\beta \geq 1\%$, except for a level at 1926 keV, whose β feeding intensity is measured as 1.94(10)% (present work) versus 0.46% (TAGS). Following a closer check with values listed in Table IV, the appreciable difference can be resolved by exchanging the value for this level with that for the adjacent level at 2180 keV, suggesting these numbers might have

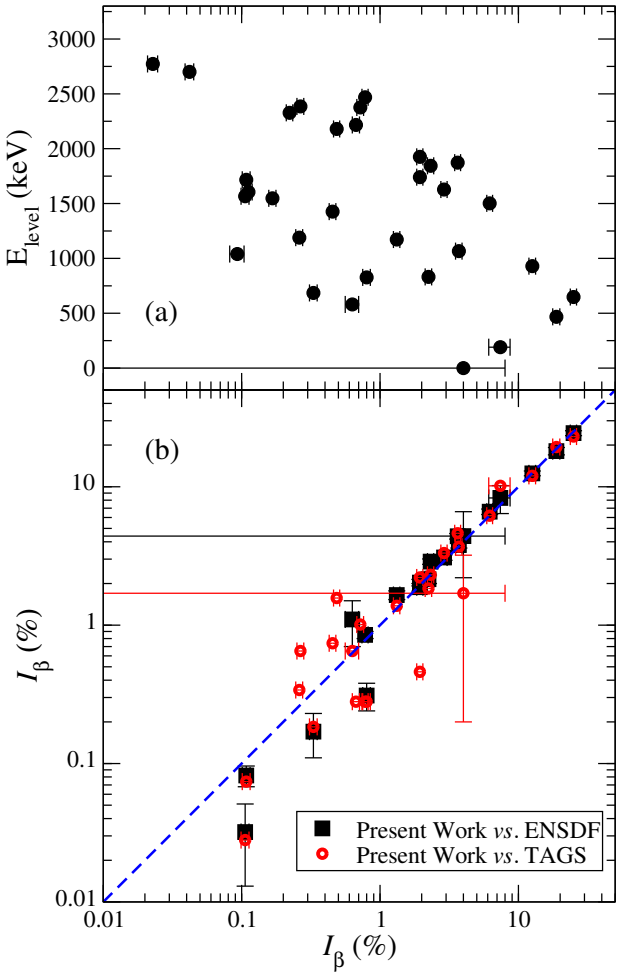

FIG. 10: (Color online) (a) Beta-feeding intensities to excited states obtained from the transition strength balance analysis in this work; and (b) comparison of β-feeding intensities from the present work with those in the evaluated data [25] also obtained from an intensity balance (solid black squares), and with the TAGS measurements by Greenwood *et al.* [9]. The blue dashed line represents the case where the compared data have the same values.

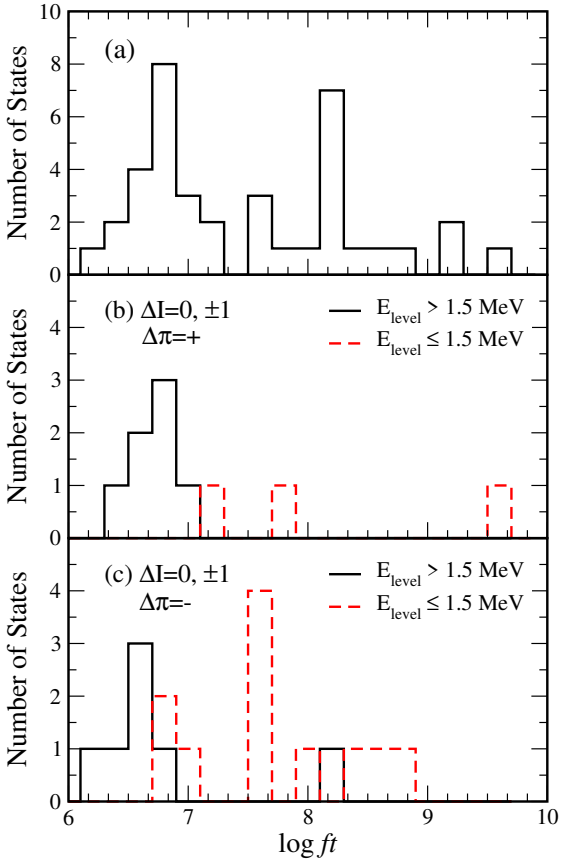

FIG. 11: (Color online) Distribution of log *ft* values from the present work for (a) all levels, (b) levels where spin changes by 0,1 with no parity change, (c) levels where spin changes by 0,1 with parity change.

been accidentally interchanged in Ref. [9].

Differences in the results of the three measurements regarding feeding strengths below 1% can be associated with differences in the sensitivities of γ-ray detection. As stated in the introduction, the accuracy of the feeding strength measured by discrete γ-ray spectroscopy suffers from the disadvantage in γ-ray detection efficiency because of the missing feedings from the undetected γ rays. On the other hand, the TAGS measurements have the advantage in efficiency, but lack of energy resolution. As a result, it is difficult to identify weakly populated states individually in this case. In most instances, only the states observed by high-resolution measurements are included in the deconvolution analysis to extract their feeding strengths. Here, the Gammasphere measurement allows improvements in both aspects with more levels identified than in earlier measurements [25], and with β-feeding intensities determined for levels with strengths two orders of magnitude smaller than was the case in Ref. [9], and also determined with well-quantified uncertainties.

However, with the advantage/disadvantage for different measurements in mind, an important issue needs to be addressed: which method is better to account for the β feeding to the ground state? Gamma decay of highly excited states associated with increased level density cannot be unambiguously detected by high-resolution γ-ray spectroscopy. As a result, these transitions are not apparent as γ-ray peaks to be included in the extraction of the ground-state feeding. In contrast, all of these transitions are properly assessed in the TAGS analysis of ground-state feeding, particularly for cases with large β-decay Q_β values, where the Pandemonium effect [8] becomes significant. Through the above comparisons with the ^{141}Ba β-decay data, the three measurements come up with consistent ground-state feeding strengths, as listed in Table IV, within the uncertainty, especially the two from discrete γ-ray spectroscopy agreeing with each other satisfactorily. Even though, in this case, the concern about the missing strength caused by Pandemonium effect is minimized due to the relative low Q_β value, the TAGS measurement quantifies the result with a better uncertainty assessment, making it an attractive option to determine the ground-state feeding, the latter being an impor-

tant quantity needed for nuclear applications.

C. Log *ft* Values

The log *ft* values are listed in Table IV along with those from the evaluated data [25]. They are computed under the condition of the ^{141}Ba ground-state property being $T_{1/2}$=18.27(7) min and Q_β= 3197 (7) keV [7]. The distribution of all log *ft* values presented in Fig. 11 is obtained by summing the states populated with a given log *ft* value. All the measured log *ft* values are in the range between 6 and 10, consistent with first-forbidden β transitions [36] without taking into account the change in spin and parity.

A group of log *ft* values centered around 6.5 is apparent in Fig. 11(a) along with an enhanced group at 8.2. It could be postulated that most of the states for the lower group can be associated with transitions to $J^\pi = 3/2^-$ states, while $\Delta\pi = -$ transitions correspond to the higher one, with the underlying assumption that allowed transitions could be well separated from first-forbidden transitions in terms of log *ft* values. However, as seen in Fig. 11(b) and (c), a similar pattern for both cases is observed, suggesting that the decay strength is influenced notably by the nuclear structure properties, beside the β-decay selection rule.

As shown in Fig. 11(c), the first-forbidden selection rule is followed for the decay to positive-parity levels with excitation energy below 1.5 MeV. The log *ft* values for $E_{level} > 1.5$ MeV are concentrated near 6.5, a value closer to that for allowed transitions. On the basis of this observation, the onset of substantial collectivity can be speculated to manifest itself above 1.5 MeV, where the configurations comprise a sizable admixture of the deformed ground-state wavefunction of ^{140}Ba, leading to significant overlap between initial and final states.

Direct population of $J^\pi = 3/2^-$ levels is expected to be through allowed transitions with log *ft* values smaller than 6 [36], but the measured values, as shown in Fig. 11(b), appear to be those for first forbidden transitions. To produce a negative-parity state within the shell-model framework in ^{141}La requires either breaking a pair of neutrons, with one of them excited across the $N = 82$ shell gap, or one proton occupying the $h_{11/2}$ orbital. In both schemes, the excitation to the final configurations are not energetically favorable. Therefore, these levels with $J^\pi = 3/2^-$ could not be interpreted in a straightforward way as single-particle states. They likely result from particle states coupled to the 1803-keV, 3^- state of the ^{140}Ba core.

Particularly, the spin and parity of the 992-keV state is assigned as $3/2^-$, and is expected to be populated by an allowed transition. However, its log *ft* value is determined to be 9.7(3), corresponding to a first-forbidden transition at its upper limit. This gives rise to concern about the J^π assignment. A J=3/2 assignment can be confirmed by the angular correlations of $801_\gamma - 190_\gamma$ (Fig. 6(f)) and $687_\gamma - 304_\gamma$ (Fig. 7(f)) transition pairs being consistent with $J = 3/2$ in a fashion similar to that of other transitions with the same assignments. In addition, it is proposed as a negative-parity state by the observation of being populated by $1/2^+$ levels without decaying to the $7/2^+$ ground state. In conclusion, the assignment of $J^\pi = 3/2^-$ to the 992-keV state is well justified. Therefore, the unexpected large log *ft* value is speculated to be due to a structure effect where the overlap between this state and ^{141}Ba ground state is small.

It has been pointed out that octupole correlations are insignificant for the properties of the 2^+ state of ^{140}Ba [37], but they are thought to play a major role in the 3^- level [18]. The 3^- level is located at 1803 keV, and the lowest positive-parity $13/2^+$ state with the same origin in ^{141}Ba is at 1341 keV. The high excitation energies prevent mixing with the ^{141}Ba ground state. As a result, being coupled to the 3^- state of ^{140}Ba, the 991-keV, $3/2^-$ state is very weakly populated by the β-decay of ^{141}Ba. It is worth noting that the decay of ^{143}Ba to the negative-parity state at similar excitation energy in ^{143}La follows the selection rules satisfactorily with a log *ft* value equal to 5.8 [38]. This situation can be interpreted as due to the fact that the lowered 3^- state with substantial octupole strength in ^{142}Ba [18] facilitates its mixing with the ^{143}Ba ground state [39].

V. CONCLUSION

Detailed and comprehensive information on the beta decay of ^{141}Ba has been acquired by gamma-ray coincidence measurements using Gammasphere, taking advantage of the availability of a short-lived radioactive beam delivered by the CARIBU facility. An updated decay scheme is established by γ-γ coincidence relationships enabling the observation of weaker γ transitions, as well as the measurement of γ-γ angular correlations. The extension of the level scheme demonstrates the need for a more sensitive and advanced spectrometer such as Gammasphere. The beta feedings were compared with the results of a Greenwood *et al.,* TAGS measurement and indicates the advantage and disadvantage of the discrete γ-ray spectroscopy and total absorption spectroscopy, respectively. Even though the level structure of ^{141}La appears complex, with rather mixed configurations, the distribution of log *ft* values indicates that the wave functions of the negative-parity states are dominated by the coupling to the 3^- state in the even-even core ^{140}Ba. The positive-parity states at lower energies can be understood as single-particle excitations, while, at higher energies, prolate deformed configurations are qualitatively prevalent.

VI. ACKNOWLEDGEMENTS

This work was sponsored by the Office of NP, Office of Science of the U.S. DOE, under Contract Nos. DE-AC02-98CH10886 (BNL) and DE-AC02-06CH11357 (ANL) and Grant Nos. DE-FG02-97ER41041 (UNC) and DE-FG02-97ER41033 (TUNL). This project was supported in part by the U.S. Department of Energy, Office of Science, Office of

TABLE IV: Level energies and beta feeding intensities (absolute intensities per 100 decays) following the decay of ^{141}Ba into excited states of ^{141}La. The beta intensities were calculated from a γ-ray intensity balance and are compared to those from Refs. [9, 25].

E(level) [keV]	J^π	Iβ^-[Present]	log ft [Present]	Iβ^- [25]	log ft [25]	Iβ^- [9]
2956.0		0.0036(8)	6.97(11)			
2808.5		0.0081(11)	7.29(7)			
2772.45		0.0228(19)	6.97(5)			
2700.36		0.042(3)	6.93(4)			
2485.8		0.0076(11)	8.21(7)			
2468.74	$5/2^{(+)}$	0.78(4)	6.24(3)	0.85(5)	6.21(3)	0.28
2385.68	$3/2^{(-)}$	0.266(15)	6.87(3)			0.65
2375.85	$3/2^{(-)}$	0.72(4)	6.46(3)			1.01
2345.2		0.0099(7)	8.38(4)			
2327.22	$3/2^{(-)}$	0.222(12)	7.06(3)			
2216.56	$1/2^{(+)}$	0.67(4)	6.77(3)			0.28
2180.38	$3/2^{(-)}$	0.486(25)	6.964(25)			1.57
1926.01	$3/2^{(-)}$	1.94(10)	6.724(25)	1.88(12)	6.74(3)	0.46
1872.60	$1/2^{(+)}$	3.64(18)	6.518(24)	4.39(20)	6.443(22)	4.61
1844.30	$3/2^{(-)}$	2.32(12)	6.749(24)	2.88(13)	6.661(22)	2.31
1740.69	$5/2^{(+)}$	1.94(10)	6.949(24)	2.03(11)	6.935(25)	2.21
1716.50		0.108(7)	8.23(3)	0.082(14)	8.36(8)	0.074
1628.16	$3/2^{(-)}$	2.90(15)	6.899(24)	3.08(14)	6.878(22)	3.32
1605.51		0.112(7)	8.34(3)			
1565.98		0.106(7)	8.40(3)	0.032(19)	8.9(3)	0.028
1547.69	$1/2^{(+)}$	0.167(10)	8.22(3)			
1501.56	$5/2^{(+)}$	6.2(3)	6.701(23)	6.6(3)	6.678(21)	6.18
1426.36	$3/2^{(-)}$	0.454(25)	7.910(25)			0.74
1188.97		0.261(15)	8.37(3)			0.34
1171.99	$1/2^{(+)}$	1.32(7)	7.678(24)	1.65(12)	7.58(4)	1.38
1066.57	$3/2^{(-)}$	3.71(20)	7.317(25)	3.79(18)	7.312(22)	3.69
1039.48	$5/2^{(+)}$	0.093(11)	8.94(6)			0
991.97	$3/2^{(-)}$	0.016(10)	9.7(3)			0
929.44	$5/2^{(+)}$	12.6(7)	6.896(25)	12.5(5)	6.903(19)	11.99
831.66	$3/2^{(+)}$	2.24(12)	7.720(24)	2.15(15)	7.74(3)	1.84
826.42	$5/2^{(+)}$	0.80(5)	8.17(3)	0.31(7)	8.59(10)	0.28
685.40	$3/2^{(+)}$	0.330(21)	8.66(3)	0.17(6)	8.95(16)	0.184
647.94	$3/2^{(+)}$	25.0(13)	6.805(24)	24.4(10)	6.819(19)	23.06
580.17	$1/2^{(+)}$	0.63(7)	8.45(5)	1.1(4)	8.21(16)	0.65
467.37	$3/2^{(+)}$	18.8(11)	7.05(3)	18.1(11)	7.07(3)	19.37
190.40	$5/2^{(+)}$	7.4(13)	7.63(8)	8.3(19)	7.58(10)	10.15
0.0	$7/2^{(+)}$	4(4)	9.4^{1u}(5)	4.4(22)	9.41^{1u}(22)	1.7(15)

Workforce Development for Teachers and Scientists (WDTS) under the Science Undergraduate Laboratory Internships Program (SULI).

[1] G.R. Keepin *et al.,* Phys. Rev. **107**, 1044 (1957).

[2] A. Algora *et al.,* Hyperfine Interactions **223**, 245 (2014).

[3] A. A. Sonzogni, T. D. Johnson, and E. A. McCutchan, Phys. Rev. C **91**, 011301 (2015).
[4] M. Estienne, M. Fallot, A. Algora, J. Briz-Monago, V.M. Bui, S. Cormon, W. Gelletly, L. Giot, V. Guadilla, D. Jordan, L. Le Meur, A. Porta, S. Rice, B. Rubio, J.L. Tain, E. Valencia, and A.-A. Zakari-Issoufou, Phys. Rev. Lett. **123**, 022502 (2019).
[5] Patrick Jaffke and Patrick Huber, Phys. Rev. Applied **8**, 034005 (2017).
[6] A. Algora *et al.,* Phys. Rev. C **68**, 034301 (2003).
[7] M. Wang, W.J. Huang, F.G. Kondev, G. Audi, and S. Naimi, Chin. Phys. C **45**, 030003 (2021).
[8] J.C. Hardy, L.C. Carrax, B. Jonson, and P.G. Hansen, Phys. Lett. B **71**, 307 (1977).
[9] R.C. Greenwood, R.G. Helmer, M.H. Putnam, and K.D. Watts, Nucl. Instrum. Methods Phys. Res. A **390**, 95 (1997).
[10] R.C. Greenwood, M.H. Putnam, and K.D. Watts, Nucl. Instrum. Methods Phys. Res. A **378**, 312 (1996).
[11] R.G. Helmer, R.C. Greenwood, K.D. Watts, and M.H. Putnam, Nucl. Instrum. Methods Phys. Res. A **339**, 189 (1994).
[12] V. Guadilla *et al.,* Phys. Rev. Lett. **122**, 042502 (2019).
[13] A. Fijalkowska *et al.,* Phys. Rev. Lett. **119**, 052503 (2017).
[14] A.C. Dombos *et al.,* Phys. Rev. C **103**, 025810 (2021).
[15] D.A. Brown *et al.,* Nucl. Data Sheets **148**, 1 (2018).
[16] A.J.M. Plompen *et al.,* Eur. Phys. J. A **56**, 181 (2020).
[17] A.C. Mueller, F. Buchinger, W. Klempt, E.W. Otten, R. Neugart, C. Ekstrom, and J. Heinemeier, Nucl. Phys. A **403**, 234 (1983).
[18] W. Urban, M. A. Jones, J. L. Durell, M. Leddy, W. R. Phillips, A. G. Smith, B. J. Varley, I. Ahmad, L. R. Morss, M. Bentaleb, E. Lubkiewicz, N. Schulz, Nucl. Phys. A **613**, 107 (1997).
[19] V. Berg, A. Hoglund, and B. Fogelberg, Nucl. Phys. A **155**, 297 (1970).
[20] L.D. McIsaac and E.L. Murri, Nucl. Phys. A **156**, 212 (1970).
[21] A.N. Proto, D. Otero, and E. Achterberg, Nucl. Phys. **5**, 121 (1979).
[22] S.H. Faller, C.A. Stone, J.D. Robertson, C. Chung, N.K. Aras, W.B. Walters, R.L. Gill, and A. Piotrowski, Phys. Rev. C **34**, 654 (1986).
[23] I. Y. Lee, Nucl. Phys. A **520**, 641c (1990).
[24] G. Savard, S. Baker, C. Davids, A. F. Levand, E. F. Moore, R. C. Pardo, R. Vondrasek, B. J. Zabransky, and G. Zinkann, Nucl. Instrum. Methods B **266**, 4086 (2008).
[25] N. Nica, Nucl. Data Sheets **122**, 1 (2014).
[26] http://www.phy.anl.gov/gammasphere/doc/index.html, 7th July 2015.
[27] D.C. Radford, Nucl. Instrum. Methods Phys. Res. A **361**, 297 (1995).
[28] M.J. Martin, Nucl. Data Sheets **114**, 1497 (2013).
[29] H. Junde, H. Su, and Y. Dong, Nucl. Data Sheets **112**, 1513 (2011).
[30] B. Singh and J. C. Roediger, Nucl. Data Sheets **111**, 2081 (2010).
[31] See supplemental material available at [URL will be inserted by publisher] for level scheme drawings for the decay of ^{141}Ba into ^{141}La.
[32] G.H. Fuller, J. Phys. Chem. Ref. Data **5**, 835 (1976)
[33] K. Wendt, S.A. Ahmad, C. Ekstrom, W. Klempt, R. Neugart, E.W. Otten, Z. Phys. **A329**, 407 (1988).
[34] T. Kibedi, T. W. Burrows, M. B. Trzhaskovskaya, P. M. Davidson, and C. W. Nestor Jr., Nucl. Instrum. Methods Phys. Res. A**589**, 202 (2008).
[35] R.J.Gehrke, Int. J. Appl. Radiat. Isotop. **32**, 377 (1981).
[36] W. Loveland, D. J. Morrissey, and G. T. Seaborg, Modern Nuclear Chemistry (Wiley, New York, 2006).
[37] C. Bauer *et al.,* Phys. Rev. C **86**, 034310 (2012).
[38] E. Browne, and J. K. Tuli, Nucl. Data Sheets **113**, 715 (2012).
[39] C. Morse *et al.*, Phys. Rev. C **102**, 054328 (2020).